Hindawi
Advances in Materials Science and Engineering
Volume 2019, Article ID 2710926, 13 pages
https://doi.org/10.1155/2019/2710926

Research Article

Adsorption of Arsenate from Aqueous Solution onto Modified Vietnamese Bentonite

Nguyen Le My Linh,[1] Duc Hoang Van,[1] Tran Duong,[1] Mai Xuan Tinh,[2] and Dinh Quang Khieu [2]

[1]*University of Education, Hue University, Hue 530000, Vietnam*
[2]*University of Sciences, Hue University, Hue 530000, Vietnam*

Correspondence should be addressed to Dinh Quang Khieu; dqkhieu@hueuni.edu.vn

Received 15 January 2019; Accepted 13 March 2019; Published 11 April 2019

Academic Editor: Frederic Dumur

In this study, pillared layered clays were prepared by modifying Vietnamese bentonite with polymeric Al and Fe. The obtained materials were characteristic of X-ray diffraction analysis, thermal analysis, and nitrogen adsorption/desorption isotherms. The results indicated that hydroxy-aluminum ($[Al_{13}O_4(OH)_{24}(H_2O)_{12}]^{7+}$) and poly-hydroxyl-Fe or polyoxo-Fe cations were intercalated into layers of clay, resulting in an increase of d_{001} values and of the specific surface areas compared with those of initial bentonite. Modified bentonites were employed to adsorb As(V) from aqueous solution. The adsorption of As(V) was strongly dependent on solution pH, and the maximum adsorption of modified bentonites was obtained in the pH 3.0 for Fe-bentonite and the pH 4.0 for Al-bentonite. The equilibrium adsorption study showed that the data were well fit by the Langmuir isotherm model. The maximum monolayer adsorption capacity of As(V) at 30°C derived from the Langmuir equation was 35.71 mg/g for Al-bentonite and 18.98 mg/g for Fe-bentonite. Adsorption kinetics, thermodynamics, and reusability of modified bentonites have been addressed.

1. Introduction

Arsenic is a potentially toxic metal that is said to be one of the most concerned contaminants in aquatic sources. Many approaches have been reported for the removal of arsenic including membrane dialysis, oxidation/reduction, precipitation/coprecipitation, filtration and adsorption, and ion exchange [1]. Among them, adsorption is recognized as one of the most promising method due to high efficiency and low cost. Various materials such as dolomite [2], chitosan [3], zeolites [4], organic clays [1], pillared interlayered clay [5, 6], activated carbon [7], metal oxides [8], and reduced metals [9] have been applied as adsorbents to eliminate arsenic from aqueous solutions. Many reports demonstrate that clays and modified clays have great potential to adsorb arsenic from contaminated water. Among the modified clays, pillared interlayered clays (PILCs) by means of the replacement of the exchangeable interlayer cations with Al_{13}, Fe_{13} Keggin ions have attracted extensive attention [10–12]. The surface area and pore volume of these PILCs are greatly enhanced so that they are used as effective adsorbents for arsenate removal. Ramesh et al. [5] reported that the maximum arsenate adsorption of Al/Fe-modified montmorillonite was about 21.23 mg/g (pH 3.0–6.0). Luengo et al. [6] studied the arsenate adsorption on a Fe(III)-modified montmorillonite. The authors concluded that both monomeric/polymeric Fe(III) species in the interlayer and on the external surface were responsible for arsenate adsorption. Zhao et al. [10] have proven that the adsorption capacity of the montmorillonites for As(V) was significantly promoted with increasing Al_{13} content. The experimental results showed the important role of the high positive charge of Al_{13} in the improvement of adsorption capacity of the modified montmorillonites. However, up to now, less efforts have been paid on both mechanism, kinetics, and thermodynamics of arsenate adsorption onto inorganic clay.

In the present article, the preparation of pillared layered clays by modification of bentonite with polymeric Al and Fe

and the removal of As(V) from aqueous solution were demonstrated.

2. Experimental

2.1. Materials. Bentonite was obtained from Vietnamese mining company and purified by the sedimentation combined with sonication and centrifugation. Aluminum chloride ($AlCl_3{\cdot}6H_2O$, 99%), ferric nitrate nonahydrate ($Fe(NO_3)_3{\cdot}9H_2O$, 99%), silver nitrate ($AgNO_3$, 98%), and sodium hydroxide (NaOH, 98%) were obtained from Guangzhou company, China. Stock solution of H_3AsO_4 100 mg/L was purchased from Merck. Chemical composition in mass analyzed by EDX of SiO_2; Al_2O_3; Fe_2O_3; TiO_2; MgO; CaO; K_2O; and Na_2O in mass is 69.1; 18.7; 4.4; 0.37; 4.19; 2.93; 0.25; and 0.07, respectively. The cation exchange capacity (CEC) was found to be 0.75 mmol/g.

2.2. Characterization. X-ray diffraction (XRD) patterns were obtained on D8-Advance Brucker, Germany with CuKα radiation. Thermogravimetric (TG) analysis was recorded on DTG-60H (Shimadzu) from 25 to 1000°C at a heating rate of 10°C/min under air atmosphere. Fourier transform infrared spectra (FTIR) were carried out on SHIMADZU FT-IR 8010M. Nitrogen adsorption/desorption isotherms were performed on Tri Star 3000. Before adsorption measurements, the specimen of 1.25 gram was outgassed for 5 h at 250°C. BET specific surface area was calculated from the nitrogen adsorption data with the relative pressure ranged from 0.04 to 0.25. Scanning electron microscopy (Hitachi, S-4500) was used to analyze the morphology of the obtained samples. A pH meter (Horiba, F-52) was employed for pH measurements. The point of zero charge (pH_{PZC}) of bentonite and polymeric Al/Fe-modified bentonite was calculated by the pH drift method. Arsenate was analyzed by means of atomic absorption spectroscopy (AAS, SHIMADZU-6800).

2.3. Preparation of Fe-Bentonite and Al-Bentonite. The purified bentonite was noted as B. The Fe pillaring solution, prepared from $Fe(NO_3){\cdot}9H_2O$ and NaOH with OH^-/Fe^{3+} molar ratio of 0.3 was stirred for 2 h and then aged in 24 h at ambient temperature. The mixture of B (1.0 g) and 100 mL of deionized water was vigorously stirred for 1 h. After that, the Fe pillaring solution was added slowly into the suspension containing the bentonite (the ratio of 10 mmol Fe/g dry bentonite); the mixture was stirred for 24 h at room temperature. The solid was separated by centrifugation and dried at 100°C for 10 h. The obtained polymeric Fe-modified bentonite was denoted as Fe-B. The Al pillaring solution was prepared by adding 0.1 M NaOH to 0.1 M $AlCl_3$ solution with vigorous stirring to obtain the $[OH^-]/[Al^{3+}]$ molar ratio of 2.4. Then, the pillaring solution was vigorously stirred for 7 h at 70°C and aged for 24 h at ambient temperature. After the aging process, the solution was slowly dropped under vigorous stirring to bentonite suspension for 24 h (24 mmol Al/g of dry bentonite). The final solid was obtained by filtration and washed with distilled water until free of chlorides (using the $AgNO_3$ test). The solid was dried at 100°C for 10 h. The obtained polymeric Al-modified bentonite was denoted as Al-B.

2.4. Adsorption Studies. Batch adsorption experiments were performed in 100 mL flask. 0.05 g of modified bentonite was added into the 100 mL flasks containing 50 mL solution with various concentrations of As(V). The pH solution was adjusted to the desired value by adding amounts of 0.01 M NaOH or 0.01 M HCl, and the bottles were shaken by magnetic stirrer for 4 h to attain equilibrium. The adsorbent was separated by centrifugation. Then, the concentration of As(V) was analyzed by the AAS method. Blank control tests were carried out for the sake of comparison.

The adsorption capacity of arsenate was calculated by using the following equation:

$$q_t = \frac{C_o - C_t}{m} \cdot V, \tag{1}$$

where q_t is the adsorption capacity of arsenate at time t, C_o (mg/L) is the initial arsenate concentration, C_t (mg/L) is the concentration of arsenate at time t, V (L) is the volume of arsenate solution used, and m (g) is the mass of the adsorbent used.

The effect of pH on arsenic adsorption was investigated in the pH ranges from 2 to 9 at ambient temperature.

For kinetic experiments, 0.2 g of adsorbent was added to 250 mL of known initial concentration in the pH = 3.0 (for the Fe-B sample) or pH = 4.0 (for the Al-B sample), and the mixture was stirred at an identical stirring speed of 600 rpm. At given time intervals, about 5 mL of solution was withdrawn and then centrifuged, and the equilibrium concentrations of the adsorbate were analyzed by the AAS method. The adsorption kinetics experiments were conducted at 10°C, 20°C, 30°C, and 40°C.

3. Results and Discussion

3.1. Characterization of the Adsorbents. The XRD patterns of B, Fe-B, and Al-B samples are shown in Figure 1.

The XRD patterns of B, Fe-B, and Al-B samples are shown in Figure 1. The basal spacing (d_{001}) of B is 1.44 nm while the recorded basal spacings were 1.48 nm for the Fe-B and 1.78 nm for the Al-B. Changes in the basal spacing depended on the charge, size, and hydration behavior of the ion or molecule that was located in the interlayer and on interactions between it and the phyllosilicate layers [12]. For the Fe-B sample, a slight increase in d_{001} has contributed to the presence of polymeric species of iron within the interlayer. In addition, from Figure 1, there was no characteristics reflections peaks of phases α, β–FeOOH, Fe_2O_3, and Fe_3O_4, showing that the iron oxides and hydroxides were not formed in Fe-bentonite sample. It was possible that iron oxides and hydroxides were forming very fine particles absorbed onto bentonite that could not be detected by XRD to destroy a part of crystal structure of bentonite, which was reflected in the decrease of intensity of d_{001} peak. The interlayer spacing distance of Al-B was 1.74 nm; this was a proof for the successful intercalation of hydroxyaluminum polycation into the

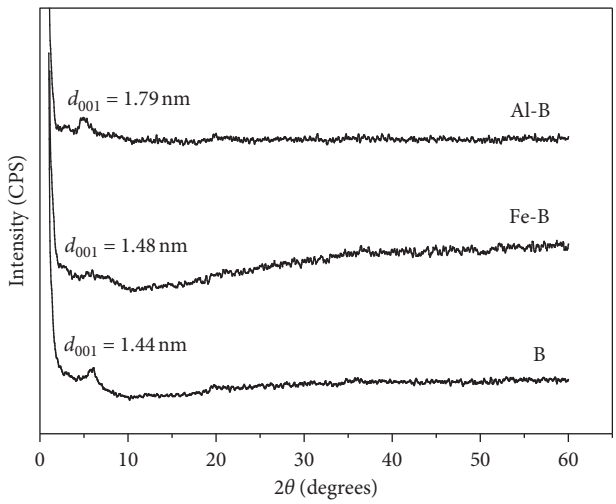

Figure 1: XRD patterns of B, Fe-B, and Al-B.

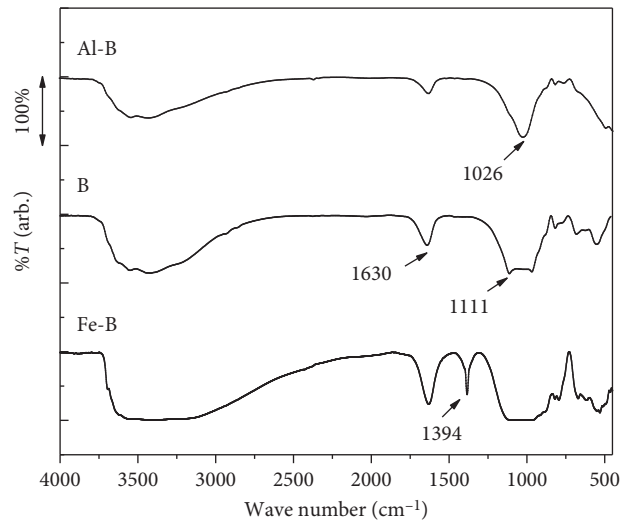

Figure 2: FTIR spectra of B, Fe-B, and Al-B.

bentonite layers. According to Hao et al. [13], the size of hydroxyaluminum polycation ($[AlO_4Al_{12}(OH)_{24}(OH_2)_{12}]^{7+}$) was of about 0.9 nm, and the basal spacing (d_{001}) of bentonite was 0.96 nm, so if there was an intercalation of ion Keggin Al_{13} into the interlayer space of bentonite, the basal spacing (d_{001}) of bentonite would be about of 1.86 nm. Other authors [14, 15] have observed that Al_{13} pillared bentonite gave basal spacings between 17 and 18 Å. This was explained by Qin et al. [11] that the value of d_{001} could not attain 1.86 nm probably due to the delamination of bentonite.

The FTIR spectra of the samples are depicted in Figure 2.

The peak at 3549 cm^{-1} of B sample was assigned to Al-Fe-OH vibration [16], the peak at 3414 cm^{-1} contributed to Fe-Fe-OH vibration [16] and HO-H vibration of the adsorbed water, and the peak at 1638 cm^{-1} was due to the deformation band (δ(O-H)) of physically adsorbed water. The peak at 1111 cm^{-1} was assigned to Si-O vibration in tetrahedral. If the amount of iron (Fe) in clays was high, this peak would shift to the higher position. According to other reports [1, 11, 17], this peak was in the range of 1033–1041 cm^{-1}, indicating that bentonite was iron-rich clay. The peak at 964 cm^{-1} was corresponded to Si-OH vibration [18], the peak at 816 cm^{-1} was because of the deformation vibration of Fe-Fe-OH [16], and the peak at 675 cm^{-1} was attributed to Al-Fe-OH vibration [19].

FT-IR spectra of the Fe-B and Al-B show that some characteristic bands of the initial bentonite were changed. Peak related to the δ(O-H) deformation shifted from 1638 cm^{-1} (B) to 1630 cm^{-1} (Fe-B) and to 1636 cm^{-1} (Al-B) with lower intensity. This could be due to the decrease of the H_2O content with replacing of the intercalated Fe/Al polycations. For Al-B, the peak at 3441 cm^{-1} and the intensity was higher than that of B (3414 cm^{-1}). The former was contributed to the O-H stretching vibration in hydroxyl-Al cations while the latter was corresponded to the hydroxyl groups in water-water hydrogen bands [17]. The band of Si-O vibration shifted from 1111 to 1026 cm^{-1} attributing to the strong interactions of the hydroxyl Al and bentonite layers. The FTIR results were in accordance with those of XRD.

TG and DTA curves of B, Fe-B, and Al-B samples are presented in Figure 3.

TG and DTA curves of B, Fe-B, and Al-B samples are presented in Figure 3. There were three main mass losses in the TG curve for the sample without modification. The first one below 200°C was due to physical water adsorption. The second mass loss being broadened from 200 to 600°C could be assigned to the interlayer water in bentonite structure. The third mass loss in the range of the temperatures over 600°C corresponding to the DTA peak 778°C was contributed to the dehydroxylation of bentonite layers. The TG curves of Fe-B and Al-B samples were similar than that of B sample. The mass loss in the range of 20–200°C (Loss 1) was assigned to physically adsorbed water. This period of the Al-B sample corresponding to the DTA endothermic peak 75°C was also attributed to the dehydration of oligomer Al cations [20], and the value was 14.1% which was higher than that of the unmodified one (3.5%). The mass loss in the range of 200–400°C (Loss 2) was contributed to the dehydration of bentonite layers and the decomposition of hydroxyl groups in polymeric Fe/Al cations. The second mass loss of Fe-B and Al-B samples at 200–400°C was 11.2% and 9.9%, respectively, which was higher than that of the B sample (8.1%). The mass loss above 600°C (Loss 3) was due to the decomposition of hydroxyl groups in the octahedron layer of bentonite.

The nitrogen adsorption and desorption isotherms of B, Fe-B, and Al-B materials are shown in Figure 4.

The nitrogen adsorption/desorption isotherms of the samples were all of type III according to IUPAC classification which indicated that the samples possessed mesoporous structure. The shape of hysteresis loops around from 0.4 to 0.9 of relative pressure was attributed to the slit-shaped pores, and their sizes are not well proportioned [4]. Table 1 lists the textural properties of all the samples. The BET surface area of pure bentonite was 114.44 m^2/g, but it increased to 146.07 m^2/g (Fe-B) and 170.13 m^2/g (Al-B) after modification. This is probably due to the increase of micropore volume (0.057 cm^3/g) and micropore surface area

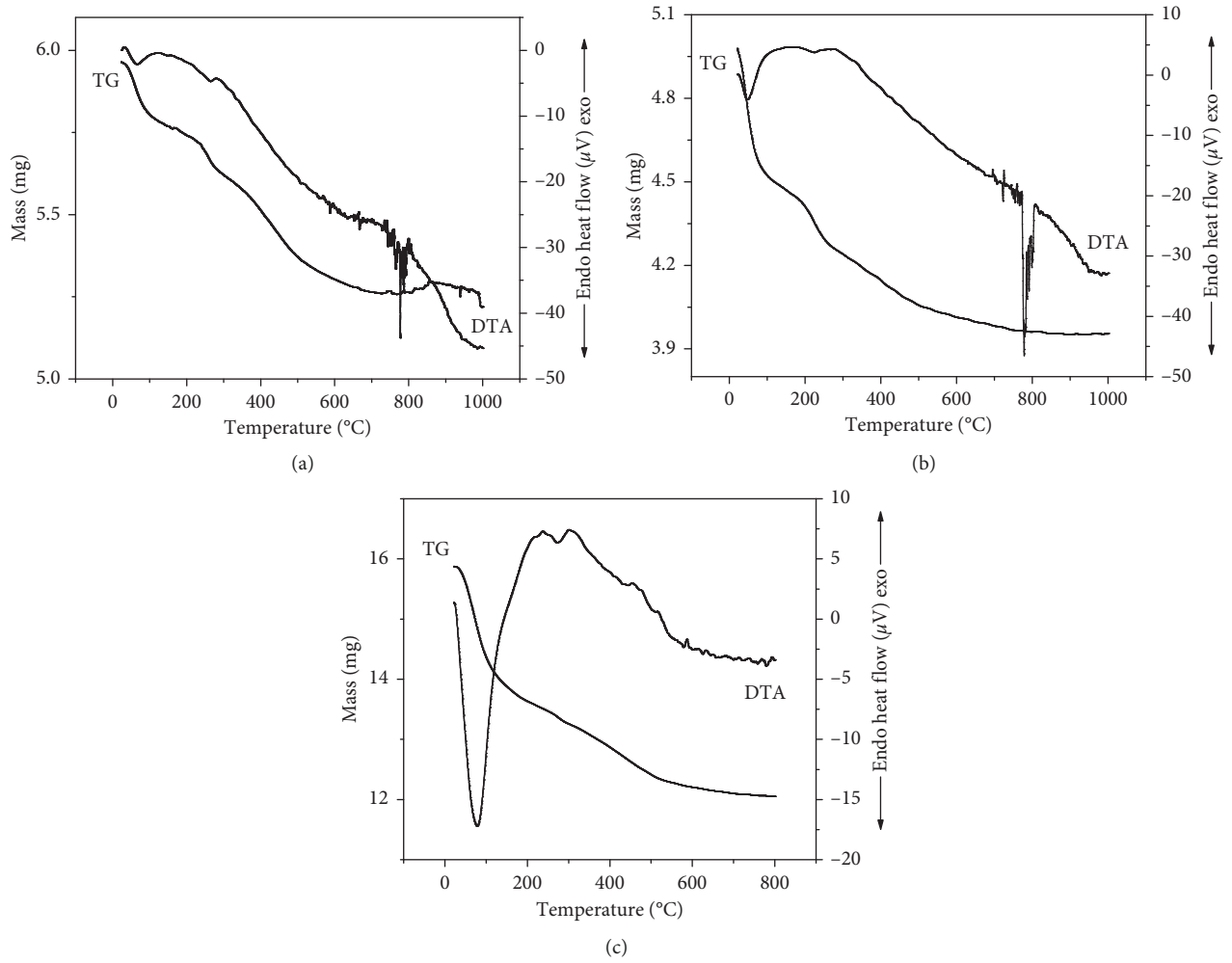

Figure 3: TG and DTA curves of B (a), Fe-B (b), and Al-B (c).

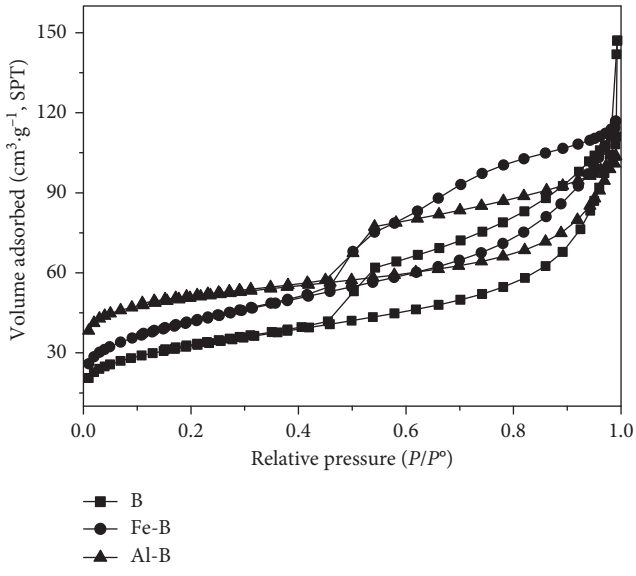

Figure 4: N_2 adsorption/desorption isotherms of B, Fe-B, and Al-B.

Table 1: Textural parameters of B, Fe-B, and Al-B samples.

Adsorbent	S_{BET} (m^2/g)	S_{micro} (m^2/g)	S_{ext} (m^2/g)	V_{micro} (cm^3/g)	V_{total} (cm^3/g)
B	114.44	44.72	69.72	0.020	0.187
Fe-B	146.07	41.03	105.04	0.018	0.159
Al-B	170.13	119.61	50.52	0.057	0.111

($119.61\ m^2/g$) in the interlayer spaces of the modified bentonite. This result was similar to the report of Ramesh et al. [5]. Before inserting polymeric Al into interlayer spaces of bentonite, these spaces were full of hydrated cations. The arrangement of these cations created the spaces between them, favoring the absorption of nitrogen. When intercalating polymeric Al into the bentonite, there were more pores in the interlayer space of bentonite favoring the absorption of nitrogen, so the micropore surface area of Al-B sample increased. According to the other authors [21, 22], the cation charge in the spaces of bentonite strongly affected the absorption of nitrogen. The decrease of external areas of

Al-B sample was explained by the increase of the number of micropores.

3.2. Adsorption Studies

3.2.1. Effect of pH. The pH effect on the arsenate adsorption capacity of polymeric Al/Fe-modified bentonite is shown in Figure 5.

It was found that the best adsorption of As(V) onto modified bentonite was in the range of pH 2.0–4.0. When increasing pH from 4.0 to 9.0, the amount of arsenate adsorbed (q_e) decreased. The point of zero charge (pH_{PZC}) of Fe-B and Al-B samples was, respectively, found to be 3.1 and 4.8 (Figure 6). At $pH < pH_{PZC}$, the modified bentonite surface was positively charged, so it favored for the adsorption of arsenic species in the form of $H_2AsO_4^-$ anions by electrostatic interaction. However, at a $pH > pH_{PZC}$, the modified surface was negatively charged, causing a repulsion force between the As(V) anions and bentonite surface. In addition, the hydroxyl ions and arsenate species could compete for adsorption at high pH causing a reduction in As(V) adsorption. Experimental results showed that As(V) had a maximum adsorption at pH 3.0 for Fe-B sample and pH 4.0 for the Al-B sample. Therefore, pH 3.0 and pH 4.0 were selected for further experiments, respectively, for Fe-B and Al-B samples.

In order to get more understanding of mechanism for arsenate absorption onto modified bentonite, the As(V) absorption at different pH was carried out. The pH values before and after the absorption are shown in Table 2.

From Table 2, it can be observed that the values of the pH for all of cases in the adsorption experiment changed. The pH values decreased after the arsenate absorption onto Fe-B. This could be explained by the reaction between the absorption sites $Fe\text{-}OH_{(surface)}$ and $H_3AsO_{4(solution)}$, creating the surface complexes such as the following:

$$Fe\text{-}OH_{(surface)} + H_3AsO_{4(solution)} \rightleftarrows Fe\text{-}HAsO_4^- + H_{(solution)}^+ + H_2O \quad (2)$$

The liberation of H^+ ions decreased pH of the solution.

The pH increased after the As(V) absorption onto Al-B sample due to the following reaction:

$$(Fe/Al) - OH_{(surface)} + H_2AsO_{4(solution)}^- \rightleftarrows (Fe/Al) - H_2AsO_{4(surface)} + OH_{(solution)}^- \quad (3)$$

The liberation of OH^- ions increased pH of the solution.

So, in this pH range, the main adsorption mechanisms could be considered as the electrostatic interactions and ion exchange.

FTIR spectra of Fe-B before and after the As(V) absorption are depicted in Figure 7.

Figure 7 shows a band in the range of 3500–3700 cm^{-1}, related to the stretching vibration of the structural hydroxyls group (AlAlOH, AlMgOH) [5]; a strong band at 3563 cm^{-1} related to the O-H stretching vibration of the silanol (Si-OH) groups and HO-H vibration of the water adsorbed silica surface [5]. The adsorption band at 1635 cm^{-1} was due to the deformation band (δ(O-H)) of physisorbed water [17]. After As(V) adsorption, these peaks were also observed with decreased intensity. This should be assigned to the direct interactions between arsenate anions and Fe-OH and Al-OH groups at corners of bentonite layers to create Fe-O-As(V) or Al-O-As(V) bonds which decreased intensity of these peaks. In addition, a new peak with low intensity was observed at 879 cm^{-1} corresponding to As-O vibration in $HAsO_4^{2-}$ anion, indicating that there was the As(V) adsorption onto Fe-B.

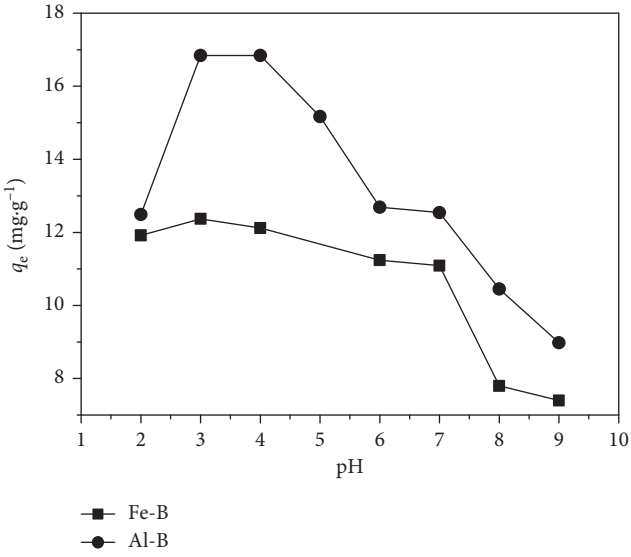

Figure 5: Effect of pH on the adsorption capacity of As(V) onto Fe-B sample ($C_{o(As)} = 12.98$ mg/L) and Al-B sample ($C_{o(As)} = 16.84$ mg/L) ($T = 303$ K, $m = 0.05$ g, $t = 4$ h).

The SEM images of Fe-B, Fe-B after the As(V) adsorption, Al-B, and Al-B after the As(V) adsorption are shown in Figure 8.

The morphology of modified bentonite changed clearly by the As(V) adsorption. The morphology of Fe-B included plates with diameter of several μm, around of which particles of small sizes were located. This morphology might facilitate for As(V) to adsorb onto modified bentonite. After As(V) adsorption, the lamellar structure of the Fe-B was left and a large number of flakes appeared. This indicated that there was a change in distance between the clay particles after arsenate adsorption. In addition, the small-size particles around the clay plates disappeared, suggesting that small clusters of Fe(III) oxides and hydroxides were also adsorption sites on surfaces. The morphology of Al-B sample consisted of the aggregate of smectites with irregular shape and partly a mass of flake shape. After arsenate adsorption, the modified clay surface was changed to an aggregated morphology, and there were several clusters around the clay plates. This indicated that the As(V) adsorption had a strong influence on the structure and morphology of modified bentonites.

3.2.2. Adsorption Kinetics. Experimental kinetic data were evaluated by using pseudo-first-order and pseudo-second-order kinetic models. The pseudo-first-order kinetic model in linear form is presented in the following equation:

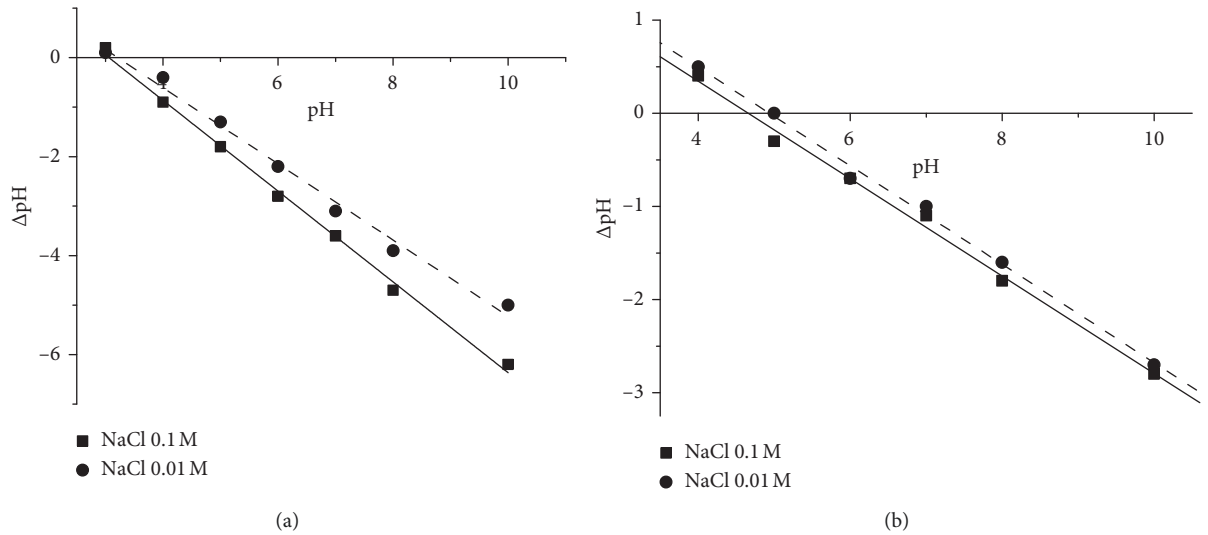

Figure 6: Point of zero charge plots of Fe-B (a) and Al-B (b).

Table 2: pH of As(V) solution before and after the arsenate absorption onto Fe-B ($C_{o(As)} = 12.98$ mg/L) and Al-B ($C_{o(As)} = 16.84$ mg/L) ($T = 303$ K, $m = 0.05$ g).

pH before the arsenate absorption	2.0	3.0	4.0	5.0	6.0	7.0	8.0	9.0
pH after the arsenate absorption onto Fe-B	2.0	2.9	3.3	—	4.0	4.8	7.0	7.2
pH after the arsenate absorption onto Al-B	2.7	3.7	5.4	5.8	6.4	7.9	8.1	9.4

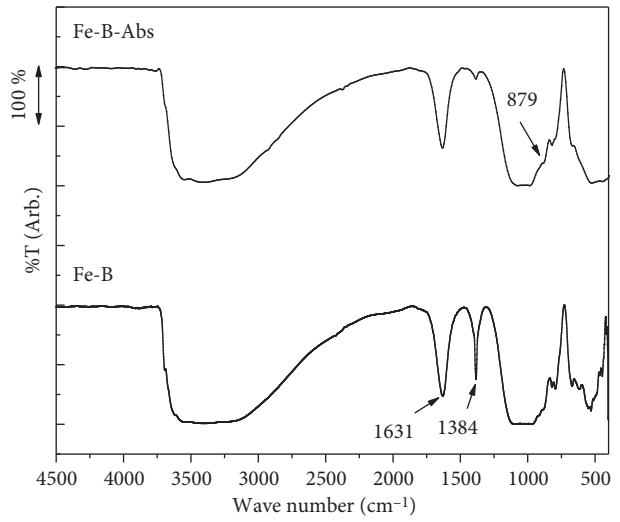

Figure 7: FT-IR spectra of Fe-B before and after the As(V) adsorption.

$$\ln(q_e - q_t) = \ln q_e - k_1 \cdot t, \tag{4}$$

where q_e and q_t are the adsorption capacity at equilibrium and at time t (mg/g) and k_1 is the pseudo-first-order rate constant (min^{-1}).

The pseudo-second-order kinetic model is given by [23, 24]

$$\frac{t}{q_t} = \frac{1}{k_2 q_e^2} + \frac{1}{q_e} \cdot t, \tag{5}$$

where k_2 is the equilibrium rate constant of pseudo-second-order kinetic model (g/mol·min).

The goodness of fit for the compatible model is assessed based on determination coefficient R^2 for the regression equation.

The plots of pseudo-first-order and pseudo-second-order kinetic models are illustrated in Figures 9 and 10, respectively. Their parameters are summarized in Table 3. The high determination coefficients (>0.92) as well as the calculated q_e values close to the experimental ones indicated that pseudo-second-order kinetic model was more suitable for the description of the adsorption kinetics of arsenate on modified bentonite (Table 3). This implied that the adsorption process could be chemisorption [23, 24]. The values of q_e at different temperatures for Al-B were greater than those for Fe-B, indicating that the adsorption capacity of Al-B is larger than that of Fe-B. The average diameter of $H_2AsO_4^-$ ions was about 3.5 Å, meanwhile the pore diameter of studied materials was about 26–220 Å, so arsenate ions were easy to move inside the mesopores of materials without being obstructed the geometry.

Table 3 shows that the value of k_2 increased with increasing temperature for both two samples (Fe-B: $0.353.10^{-3}$–$7.301.10^{-3}$ g/mg·min; Al-B: $2.8.10^{-3}$–$5.8.10^{-3}$ g/mg·min).

The activation energy can be computed by using the Arrhenius equation:

$$\ln k_2 = -\frac{E_a}{RT} + \ln A, \tag{6}$$

where A is the Arrhenius constant (g/mg·min), E_a the activation energy of adsorption (kJ/mol), R is the gas constant (8.314 J/mol·K), and T is the absolute temperature (K). The activation energy (E_a) was obtained from the slope of the linear plot of ln k_2 versus $1/T$ (Figure 11(a)).

Besides calculating the activation energy, the Gibbs energy $\Delta G^{\#}$, enthalpy $\Delta H^{\#}$, and entropy $\Delta S^{\#}$ of the activation

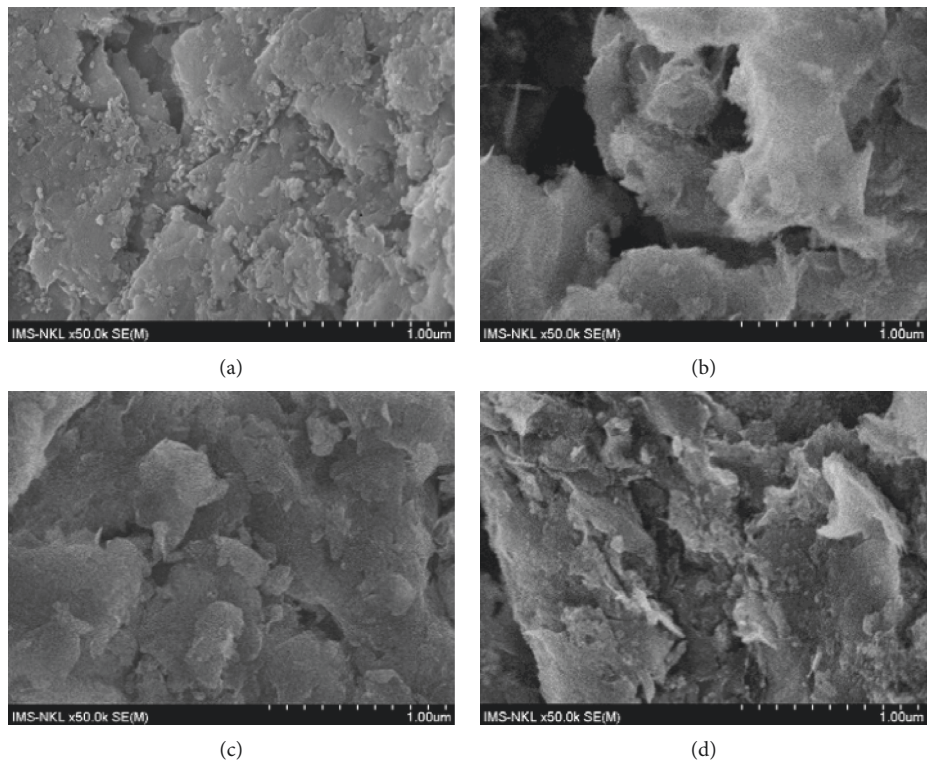

Figure 8: SEM images of Fe-B (a), Fe-B after the As(V) adsorption (b), Al-B (c), and Al-B after the As(V) adsorption (d).

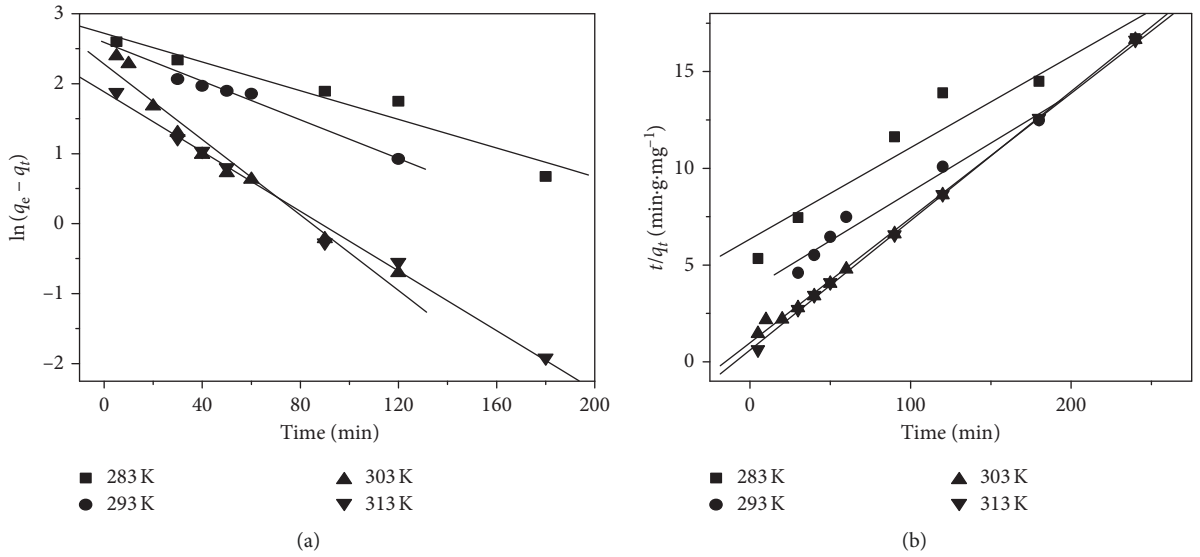

Figure 9: The pseudo-first-order kinetic model (a) and pseudo-second-order kinetic model (b) of As(V) adsorption by Fe-B at different temperatures.

for As(V) adsorption kinetics can be computed by using the Eyring equation [25]:

$$\ln \frac{k_2}{T} = \ln\left(\frac{k_b}{h}\right) - \frac{\Delta G^{\#}}{R \cdot T} = -\frac{\Delta H^{\#}}{R} \cdot \frac{1}{T} + \left[\ln\left(\frac{k_b}{h}\right) + \frac{\Delta S^{\#}}{R}\right], \quad (7)$$

where k_b (1.3807×10^{-23} J/K) is the Boltzmann constant, h (6.621×10^{-34} J·s) is the Planck constant, $\Delta G^{\#}$ is the Gibbs energy of activation, $\Delta H^{\#}$ is the activation enthalpy, and $\Delta S^{\#}$ is the activation entropy.

The linear plot of $\ln(k/T)$ versus $1/T$ gives a straight line. The activation parameters could be derived from the slope and intercepts of these lines (Figure 11(b)).

The values of the activation energy were found to be 80.29 kJ/mol and 41.90 kJ/mol for the arsenate adsorption onto Fe-B and Al-B, respectively (Table 4). The magnitude of activation energy can give information on whether the

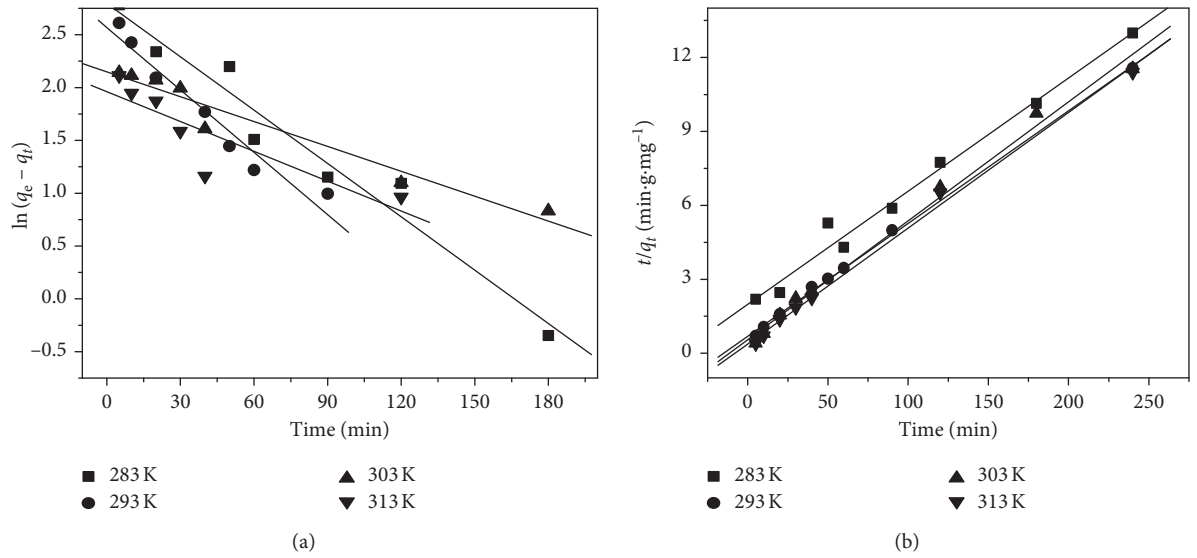

Figure 10: The pseudo-first-order kinetic model (a) and pseudo-second-order kinetic model (b) of As(V) adsorption by Al-B at different temperatures.

Table 3: Parameters of pseudo-first-order and pseudo-second-order kinetic model of As(V) adsorption by Fe-B and Al-B at different temperatures.

Adsorbent	T (K)	q_e (experimental) (mg/g)	First-order kinetic model			Second-order kinetic model		
			k_1 (min^{-1})	q_e (cal) (mg/g)	R^2	k_2 (g/mg·min)	q_e (cal) (mg/g)	R^2
Fe-B	283	14.38	0.010	15.19	0.942	0.35×10^{-3}	21.14	0.924
	293	14.42	0.013	12.44	0.977	0.68×10^{-3}	19.80	0.973
	303	14.42	0.027	9.80	0.962	4.20×10^{-3}	15.53	0.999
	313	14.44	0.021	6.57	0.992	7.30×10^{-3}	14.97	0.998
Al-B	283	18.47	1.6×10^{-3}	16.35	0.956	1.0×10^{-3}	22.22	0.984
	293	20.75	1.9×10^{-3}	13.01	0.948	2.9×10^{-3}	22.22	0.998
	303	20.80	7.0×10^{-3}	8.56	0.949	4.2×10^{-3}	20.83	0.992
	313	21.05	9.0×10^{-3}	7.09	0.752	5.8×10^{-3}	21.28	0.996

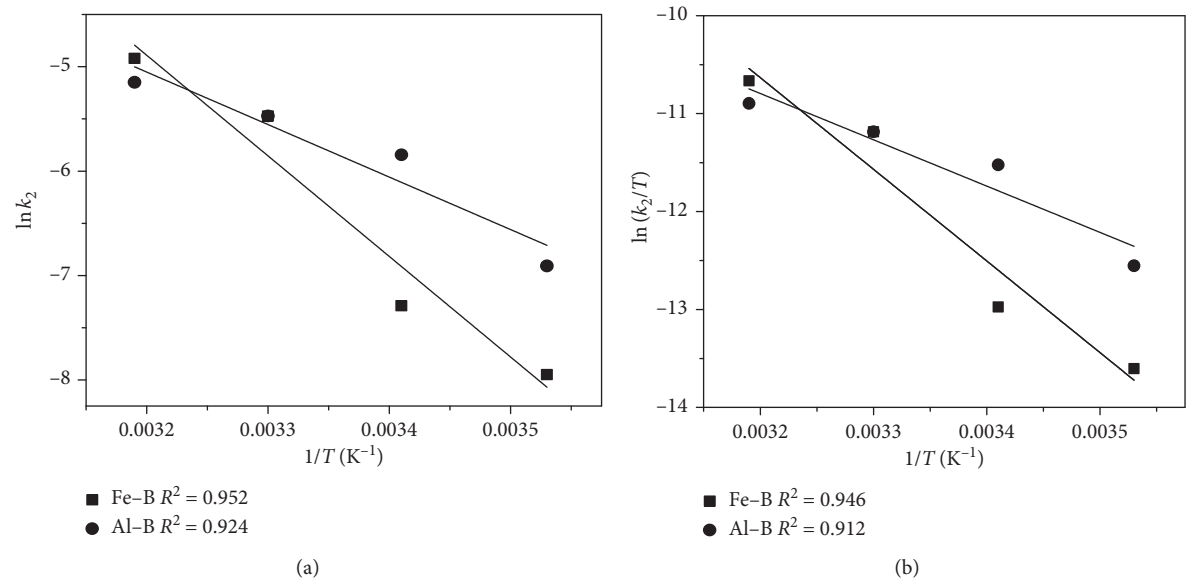

Figure 11: (a) Arrhenius plots and (b) Eyring plots of As(V) adsorption onto Fe-B and Al-B.

Table 4: Activation energy and activation parameters of adsorption process.

T (K)	E_a (kJ/mol)	$\Delta H^{\#}$ (kJ/mol)	$\Delta S^{\#}$ (kJ/mol.K)	$\Delta G^{\#}$ (kJ/mol)
Fe-B				
283	80.29	77.82	−0.037	88.41
293				88.79
303				89.16
313				89.53
Al-B				
	41.90	39.32	−0.162	85.16
				86.78
				88.40
				90.02

adsorption process is physical or chemical. Ramesh et al. [5] reported that the activation energy of physisorption was normally not more than 42 kJ/mol. Hence, the values of activation energy were found in this study suggesting that the adsorption of As(V) on Fe-B was a chemical adsorption. The smaller E_a for the adsorption of As(V) on Al-B was due to the formation of weak chemical bond between absorbent and adsorbate. According to the literature, the rate constant increased when decreasing the value of activation energy or increasing the frequency factor A. The calculated A values were found to be 1.8×10^{-11} and 80821 for the adsorption of As(V) on Fe-B and on Al-B, respectively. These results were interesting due to showing "the compensation effect" in heterogeneous adsorption.

The free energy of activation ($\Delta G^{\#}$), activation enthalpy ($\Delta H^{\#}$), and activation entropy ($\Delta S^{\#}$) are listed in Table 4. The positive value of $\Delta H^{\#}$ for both samples confirmed an endothermic process. The magnitude and sign of $\Delta S^{\#}$ can give an indication of whether the adsorption reaction is an associative or dissociative mechanism [25]. The high negative values of $\Delta S^{\#}$ manifested that the As(V) adsorption process was an associative mechanism. This was additional evidence for the analysis of adsorption mechanism as described in Section 3.2.1. The large positive values of $\Delta G^{\#}$ inferred that the adsorption reactions required energy to convert the reactants into products [26].

3.2.3. Adsorption Isotherms. Equilibrium studies were carried out to obtain the adsorption capacity of modified bentonite at different temperatures. Two adsorption isotherms, namely, the Langmuir [23] and the Freundlich [23] isotherms were employed to analyze the adsorption data. The linear form of Langmuir isotherm is given by

$$\frac{C_e}{q_e} = \frac{C_e}{q_m} + \frac{1}{K_L \cdot q_m}, \tag{8}$$

where q_e is the equilibrium adsorption capacity (mg/g), C_e is the equilibrium arsenate concentration in solution (mg/L), q_m is the monolayer adsorption capacity of the adsorbent (mg/g), and K_L is the Langmuir constant (L/mg) which is related to the energy of adsorption, respectively. q_m and K_L can be computed from the intercept and slope of the linear plot, with C_e/q_e versus C_e.

In addition, a separation factor, R_L (also equilibrium parameter), is defined by the following equation:

$$R_L = \frac{1}{1 + K_L C_i}, \tag{9}$$

where C_i (mg/L) is the initial dye concentration and K_L (L/mg) is the Langmuir constant. The value of R_L indicates the shape of the isotherms to be either unfavorable ($R_L > 1$), linear ($R_L = 1$), favorable ($0 < R_L < 1$), or irreversible ($R_L = 0$).

The Freundlich isotherm was applied to the adsorption on a heterogeneous surface with uniform energy. The linear form of this model can be expressed as follows:

$$\ln q_e = \ln K_F + \frac{1}{n} \cdot \ln C_e, \tag{10}$$

where q_e and C_e are the equilibrium adsorption capacity (mg/g) and equilibrium concentration in liquid phases (mg/L), respectively. K_F and n are the Freundlich constants which are related to adsorption capacity and intensity, respectively. The linear plot with $\ln q_e$ versus $\ln C_e$ can provide the values of K_F and n from the slope and intercepts.

The plots for he Langmuir and Freundlich isotherm models are shown in Figures 12 and 13.

As seen from Table 5, the high values of R^2 for the Langmuir isotherm model ($R^2 > 0.920$), as compared with those for the Freundlich isotherm model ($R^2 < 0.875$) and the values of R_L in the range 0 and 1 inferred that As(V) adsorption onto the modified bentonite was favorable for the Langmuir model. Based on the maximum monolayer adsorption capacity of the adsorbent q_m (mg/g), specific area of modified bentonite can computed by the following expression:

$$S = \frac{q_{max}^{As}}{M_{As}} \cdot N_A \cdot \sigma_{As}, \tag{11}$$

where q_{max}^{As} is the Langmuir monolayer adsorption capacity, M_{As} is the molar masse of As, N_A is Avogadro number, and σ_{As} is the surface area of AsO_4^{3-} ($\sigma_{As} = \pi \cdot r^2$, $r = 1.7$ Å).

Specific surface area of modified bentonite was calculated at the temperature of 283 K as follows:

$$\begin{aligned} S(\text{Fe} - \text{B}) &= \left(\frac{17.76}{75}\right) \times 6.03 \times 10^{23} \times 3.14 \times (1.7)^2 \times \left(10^{-10}\right)^2 \\ &= 12.96\ \text{m}^2/\text{g}, \\ S(\text{Al} - \text{B}) &= \left(\frac{29.41}{75}\right) \times 6.03 \times 10^{23} \times 3.14 \times (1.7)^2 \times \left(10^{-10}\right)^2 \\ &= 21.46\ \text{m}^2/\text{g}. \end{aligned} \tag{12}$$

The effective surface area values of the studied samples were less than S_{BET} of Fe-B (146.07 m^2/g) and Al-B (170.13 m^2/g), indicating that the As(V) absorption onto studied materials only occurred at the outer surfaces and in the large pores of bentonite particles.

The maximum As(V) adsorption capacities (q_m) computed from the Langmuir model at 303 K were 18.98 mg/g for Fe-B and 35.71 mg/g for Al-B. As can be seen from Table 6, the adsorption capacity for arsenate

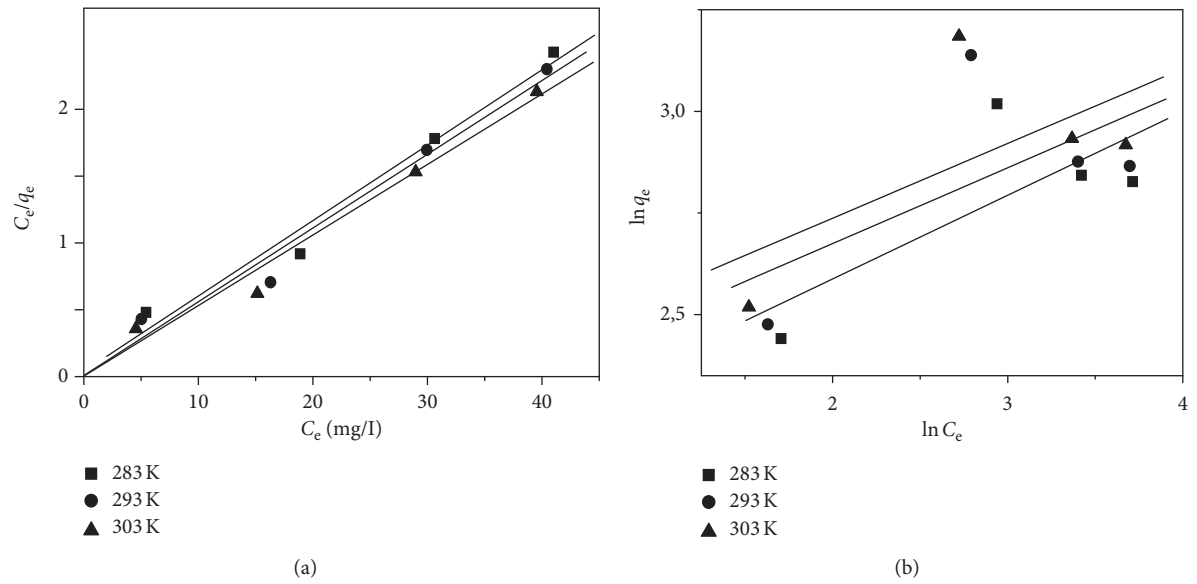

Figure 12: Plots of Langmuir (a) and Freundlich (b) isotherms in linear form for the adsorption of As(V) onto Fe-B at several temperatures.

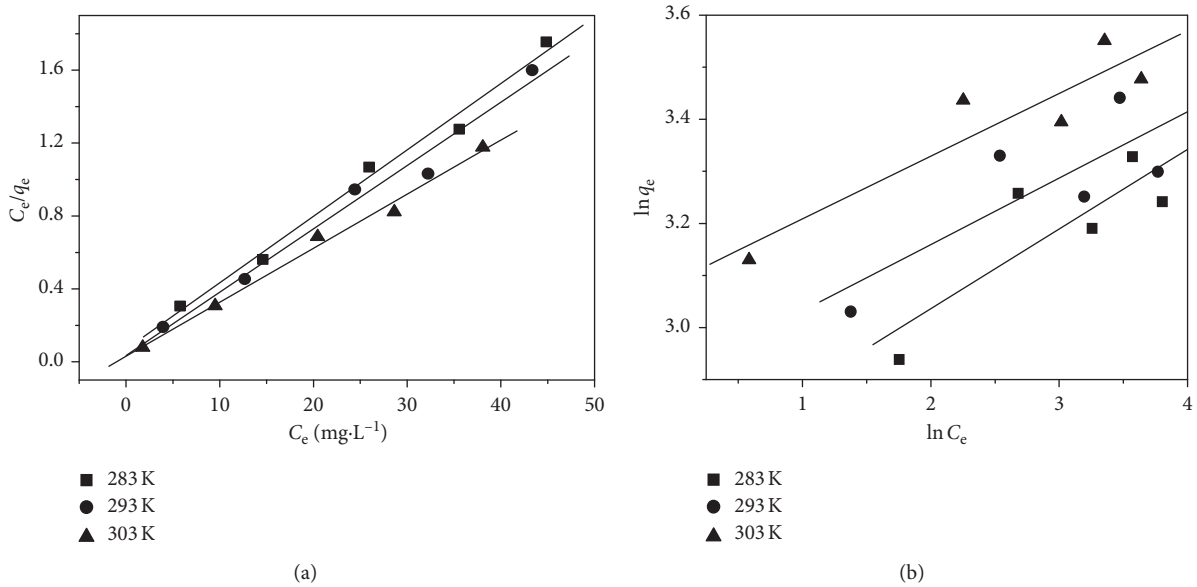

Figure 13: Plots of Langmuir (a) and Freundlich (b) isotherms in linear form for the adsorption of As(V) onto Al-B at several temperatures.

Table 5: The parameters of isotherm models in linear form for the adsorption of As(V) onto modified bentonite.

T (K)	Langmuir model				Freundlich model		
	q_{max} (mg/g)	K_L (L/mg)	R^2	R_L	K_F (mg/g)	n	R^2
Fe-B							
283	17.76	1.08	0.976	0.016–0.053	8.81	4.86	0.561
293	18.05	5.18	0.972	0.003–0.011	9.99	5.36	0.391
303	18.98	7.87	0.976	0.002–0.007	10.69	5.44	0.405
Al-B							
283	29.41	0.32	0.984	0.046–0.111	21.477	7.41	0.795
293	32.59	0.41	0.970	0.037–0.090	16.912	6.10	0.779
303	35.71	0.70	0.984	0.022–0.055	14.069	5.29	0.875

Table 6: Comparison of adsorption capacity with other adsorbents.

Adsorbent	Arsenate adsorption capacity (mg/g)	References
SMB3	0.288	[1]
Polymeric Al/Fe-modified montmorillonite	21.233	[5]
Al_{13}-Mont	5.008	[10]
C-Fe-M	8.85	[27]
Fe-M	15.15	[27]
Al-B	35.71	Present study
Fe-B	18.98	Present study

adsorption onto studied materials was greater than those for other adsorbents reported. Therefore, the modified bentonite showed a good capability for eliminating arsenate from aqueous solution down to part per billion levels, making the present modified bentonite to be used commercially in future for adsorbing arsenate from aquatic sources contaminated with arsenic.

3.2.4. Calculation of Thermodynamic Parameters. Gibb's free energy (ΔG°), entropy change (ΔS°), and enthalpy change (ΔH°) have been obtained from the following expressions [28]:

$$\Delta G^\circ = -RT \ln K_L, \tag{13}$$

where K_L is the Langmuir constant:

$$\ln K_L = -\frac{\Delta G^\circ}{RT} = -\frac{\Delta H^\circ}{RT} + \frac{\Delta S^\circ}{R}. \tag{14}$$

The values of ΔH° and ΔS° were computed from the slope and intercept of the plot, with $\ln K_L$ versus $1/T$ in Figure 14. The thermodynamic parameters for the As(V) adsorption are presented in Table 7.

For the both cases, the obtained ΔH° values were positive, which manifested the endothermic nature of arsenate adsorption onto modified bentonite. The positive value of ΔS° indicated the entropy of the system increased during the adsorption. This result suggested that the arsenate adsorption onto modified bentonite was promoted by entropy than by enthalpy. The mechanism of the As(V) adsorption onto modified bentonites might be ion exchange, so the large value of entropy was corresponded to greater randomness. The values of ΔG° were negative for both samples indicating the spontaneous adsorption in the investigated temperature range, and the decrease of ΔG° values with increasing temperature inferred that the adsorption became more favorable at higher temperature.

3.3. Reusability. In the reusability test, 0.5 g of used modified bentonites saturated with As(V) (initial Al-B or initial Fe-B) was added into thirty milliliters of 0.01 M HCl solution. The mixture was shaken at a temperature of 30°C using a magnetic stirrer for 24 h. The solids were centrifuged, rinsed for several times with distilled water, dried at 100°C, and investigated for As(V) adsorption capacity at the first run.

Figure 15 represents the reusability of modified bentonite. The adsorption capacity of the adsorbents decreased gradually during the repeated absorption/desorption operations. The adsorption capacity of Al-B decreased from 21.05 mg/g for initial adsorbent to 14.66 mg/g for third cycle. The adsorption capacity for Fe-B decreased from 14.44 mg/g for initial adsorbent to 9.98 mg/g for third cycle.

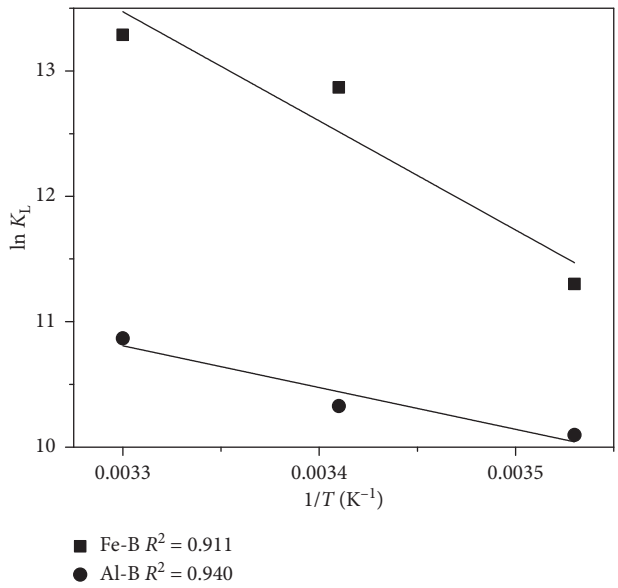

Figure 14: Plot $\ln K_L$ versus $1/T$ for the determination of thermodynamic parameters.

Table 7: Thermodynamic parameters for the As(V) adsorption onto Fe-B and Al-B materials.

Adsorbent	ΔG° (kJ/mol)			ΔH°	ΔS°
	283 K	293 K	303 K	(kJ/mol)	(kJ/mol.K)
Fe-B	−26.59	−31.35	−33.47	71.23	0.347
Al-B	−23.76	−25.16	−27.38	27.34	0.180

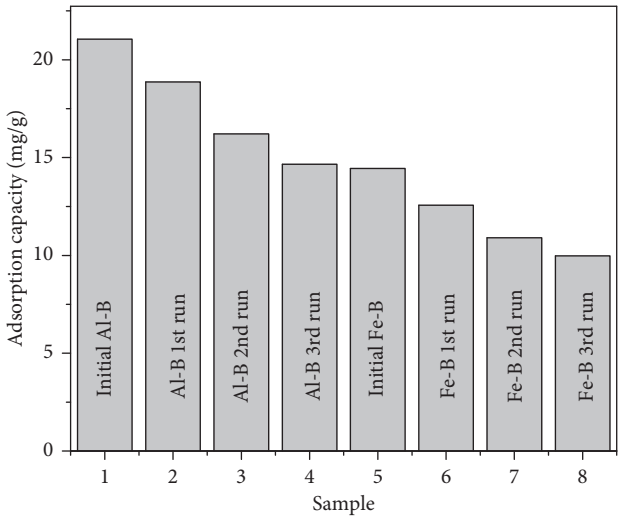

Figure 15: The dependence of adsorption capacity through the reuse of adsorbent ($C_{o(As)}$ = 24.66 mg/L, T = 303 K, m = 0.05 g, t = 4 h).

The adsorption capacity was reduced by 30.4% for Al-B and by 30.9% for Fe-B after four uses. The results showed that the polymeric Al and polymeric Fe bentonite were good reusable adsorbents in removal of arsenate ions from aqueous solution.

4. Conclusions

In this study, the polymeric Al- and Fe-modified bentonites were applied to remove arsenate ions from aqueous solution. The pseudo-second-order kinetic model fit well with the arsenate adsorption kinetic data for the two modified bentonites. The maximum monolayer adsorption capacities of As(V) at 303 K derived from the Langmuir model were 35.71 mg/g for Al-bentonite and 18.98 mg/g for Fe-bentonite, which were higher than that compared to other adsorbents reported previously. The negative values of ΔG° implied the spontaneity while the positive values of ΔH° and ΔS° indicated the endothermic nature and increase in randomness of the process taking place, respectively. The activation energies for the Fe-modified bentonite and Al-modified bentonite were found to be 80.29 and 41.90 kJ/mol, respectively. The modified bentonites can be regenerated and used effectively after four uses for adsorbing arsenate from aqueous solution.

Data Availability

The data used to support the findings of this study are available from the corresponding author upon request.

Conflicts of Interest

The authors declare that they have no conflicts of interest.

References

[1] J. Su, H.-G. Huang, X.-Y. Jin, X.-Q. Lu, and Z.-L. Chen, "Synthesis, characterization and kinetic of a surfactant-modified bentonite used to remove As(III) and As(V) from aqueous solution," *Journal of Hazardous Materials*, vol. 185, no. 1, pp. 63–70, 2011.

[2] Y. Salameh, N. Al-Lagtah, M. N. M. Ahmad, S. J. Allen, and G. M. Walker, "Kinetic and thermodynamic investigations on arsenic adsorption onto dolomitic sorbents," *Chemical Engineering Journal*, vol. 160, no. 2, pp. 440–446, 2010.

[3] K. C. M. Kwok, L. F. Koong, T. Al Ansari, and G. McKay, "Adsorption/desorption of arsenite and arsenate on chitosan and nanochitosan," *Environmental Science and Pollution Research*, vol. 25, no. 15, pp. 14734–14742, 2018.

[4] P. Chutia, S. Kato, T. Kojima, and S. Satokawa, "Arsenic adsorption from aqueous solution on synthetic zeolites," *Journal of Hazardous Materials*, vol. 162, no. 1, pp. 440–447, 2009.

[5] A. Ramesh, H. Hasegawa, T. Maki, and K. Ueda, "Adsorption of inorganic and organic arsenic from aqueous solutions by polymeric Al/Fe modified montmorillonite," *Separation and Purification Technology*, vol. 56, no. 1, pp. 90–100, 2007.

[6] C. Luengo, V. Puccia, and M. Avena, "Arsenate adsorption and desorption kinetics on a Fe(III)-modified montmorillonite," *Journal of Hazardous Materials*, vol. 186, no. 2-3, pp. 1713–1719, 2011.

[7] D. Borah, S. Satokawa, S. Kato, and T. Kojima, "Sorption of As(V) from aqueous solution using acid modified carbon black," *Journal of Hazardous Materials*, vol. 162, no. 2-3, pp. 1269–1277, 2009.

[8] M. Jang, S.-H. Min, T.-H. Kim, and J. K. Park, "Removal of arsenite and arsenate using hydrous ferric oxide incorporated into naturally occurring porous diatomite," *Environmental Science & Technology*, vol. 40, no. 5, pp. 1636–1643, 2006.

[9] S. Bang, G. Korfiatis, and X. Meng, "Removal of arsenic from water by zero-valent iron," *Journal of Hazardous Materials*, vol. 121, no. 1–3, pp. 61–67, 2005.

[10] S. Zhao, C. Feng, X. Huang, B. Li, J. Niu, and Z. Shen, "Role of uniform pore structure and high positive charges in the arsenate adsorption performance of Al13-modified montmorillonite," *Journal of Hazardous Materials*, vol. 203-204, pp. 317–325, 2012.

[11] Z. Qin, P. Yuan, J. Zhu, H. He, D. Liu, and S. Yang, "Influences of thermal pretreatment temperature and solvent on the organosilane modification of Al_{13}-intercalated/Al-pillared montmorillonite," *Applied Clay Science*, vol. 50, no. 4, pp. 546–553, 2010.

[12] L. Borgnino, M. J. Avena, and C. P. De Pauli, "Synthesis and characterization of Fe(III)-montmorillonites for phosphate adsorption," *Colloids and Surfaces A: Physicochemical and Engineering Aspects*, vol. 341, no. 1-3, pp. 46–52, 2009.

[13] Y.-F. Hao, L.-G. Yan, H.-Q. Yu et al., "Comparative study on adsorption of basic and acid dyes by hydroxy-aluminum pillared bentonite," *Journal of Molecular Liquids*, vol. 199, pp. 202–207, 2014.

[14] F. Bertella and S. B. C. Pergher, "Pillaring of bentonite clay with Al and Co," *Microporous and Mesoporous Materials*, vol. 201, pp. 116–123, 2015.

[15] M. Altunlu and S. Yapar, "Effect of OH^-/Al^{3+} and Al^{3+}/clay ratios on the adsorption properties of Al-pillared bentonites," *Colloids and Surfaces A: Physicochemical and Engineering Aspects*, vol. 306, no. 1–3, pp. 88–94, 2007.

[16] R. L. Frost and J. T. Kloprogge, "Vibrational spectroscopy of ferruginous smectite and nontronite," *Spectrochimica Acta Part A: Molecular and Biomolecular Spectroscopy*, vol. 56, no. 11, pp. 2177–2189, 2000.

[17] W. Xue, H. He, J. Zhu, and P. Yuan, "FTIR investigation of CTAB-Al-montmorillonite complexes," *Spectrochimica Acta Part A: Molecular and Biomolecular Spectroscopy*, vol. 67, no. 3-4, pp. 1030–1036, 2007.

[18] B. A. Goodman, J. D. Russell, and A. R. Frasera, "A MÖssbauer and I.R. Spectroscopic study of the structure of nontronite," *Clays and Clay Minerals*, vol. 24, no. 2, pp. 53–59, 1976.

[19] J. D. Russel and A. R. Fraser, "Infrared methods," in *Clay Mineralogy, Spectroscopic and Chemical Determinative Methods*, M. J. Wilson, Ed., pp. 11–67, Chapman & Hall, London, UK, 1994.

[20] M. E. R. J. Jalil, R. S. Vieira, D. Azevedo, M. Baschini, and K. Sapag, "Improvement in the adsorption of thiabendazole by using aluminum pillared clays," *Applied Clay Science*, vol. 71, pp. 55–63, 2013.

[21] H. Faghihian and M. H. Mohammadi, "Surface properties of pillared acid-activated bentonite as catalyst for selective production of linear alkylbenzene," *Applied Surface Science*, vol. 264, pp. 492–499, 2013.

[22] H. Khalaf, O. Bouras, and V. Perrichon, "Synthesis and characterization of Al-pillared and cationic surfactant modified Al-pillared Algerian bentonite," *Microporous Materials*, vol. 8, no. 3-4, pp. 141–150, 1997.

[23] M. E. Pena, G. P. Korfiatis, M. Patel, L. Lippincott, and X. Meng, "Adsorption of As(V) and As(III) by nanocrystalline titanium dioxide," *Water Research*, vol. 39, no. 11, pp. 2327–2337, 2005.

[24] M. Toor and B. Jin, "Adsorption characteristics, isotherm, kinetics, and diffusion of modified natural bentonite for removing diazo dye," *Chemical Engineering Journal*, vol. 187, pp. 79–88, 2012.

[25] K. A. Krishnan and T. S. Anirudhan, "Uptake of heavy metals in batch systems by sulfurized steam activated carbon prepared from sugarcane bagasse pith," *Industrial & Engineering Chemistry Research*, vol. 41, no. 20, pp. 5085–5093, 2002.

[26] H. T. M. Thanh, T. T. T. Phuong, P. L. T. Hang, T. T. T. Toan, T. X. Mau, and D. Q. Khieu, "Comparative study of Pb(II) adsorption onto MIL–101 and Fe–MIL–101 from aqueous solutions," *Journal of Environmental Chemical Engineering*, vol. 6, no. 4, pp. 4093–4102, 2018.

[27] X. Ren, Z. Zhang, H. Luo et al., "Adsorption of arsenic on modified montmorillonite," *Applied Clay Science*, vol. 97-98, pp. 17–23, 2014.

[28] A. Özcan, Ç. Ömeroğlu, Y. Erdoğan, and A. S. Özcan, "Modification of bentonite with a cationic surfactant: an adsorption study of textile dye Reactive Blue 19," *Journal of Hazardous Materials*, vol. 140, no. 1-2, pp. 173–179, 2007.